Inorganic Chemistry

Article

pubs.acs.org/IC

Atmosphere- and Voltage-Dependent Electronic Conductivity of Oxide-Ion-Conducting $Zr_{1-x}Y_xO_{2-x/2}$ Ceramics

Marc Jovaní,[†] Héctor Beltrán-Mir,*[,†] Eloisa Cordoncillo,[†] and Anthony R. West[‡]

[†]Departamento de Química Inorgánica y Orgánica, Universidad Jaume I, Avenida Sos Baynat s/n, Castellón 12071, Spain

[‡]Department of Materials Science & Engineering, University of Sheffield, Mappin Street, Sheffield S1 3JD, U.K.

ABSTRACT: Cubic, fluorite-structured solid solutions $Zr_{1-x}Y_xO_{2-x/2}$ (YSZ; x = 0.4−0.7) were prepared by sol−gel synthesis. Impedance measurements on pellets of 85% approximate density sintered at 1300 °C for 24 h showed strong evidence of oxide ion conduction with an inclined Warburg spike at low frequencies and capacitance values of ~10^{-6} F cm^{-1} at 40 Hz. Arrhenius plots of total pellet conductivities were linear with activation energies of 1.4−1.56 eV. The conductivity decreased with x and was 2−4 orders of magnitude lower than that with optimized YSZ, x = 0.08. When the atmosphere was changed from N_2 to O_2 during impedance measurements, two reversible effects were seen: the Warburg spike contracted greatly, and the sample resistance decreased. These effects were more noticeable at higher x and are attributed to the introduction of p-type electronic conduction, in parallel with the preexisting oxide ion conduction. A similar reversible result was observed upon application of a direct-current (dc) bias during impedance measurements. When either pO_2 is increased or a dc bias is applied, hole creation is believed to arise by the ionization of underbonded oxide ions situated near the Y^{3+} dopant ions. The ionized electrons are trapped at surface oxygen species, and the holes that are left on oxygen are responsible for p-type conduction. The electrolytic domain of x = 0.4−0.7 extends up to approximately 10^{-2} atm of O_2 before p-type conduction is observed. The upper pO_2 limit of the electrolytic domain of x = 0.08 is not known but is likely to be close to or slightly above 1 atm of O_2.

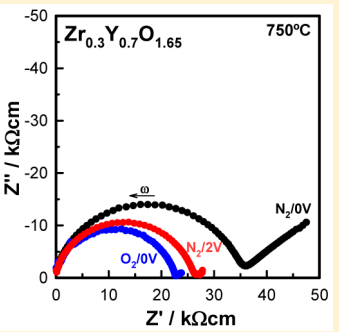

INTRODUCTION

Yttria-stabilized zirconia (YSZ) is the most widely used oxide ion conductor in solid oxide fuel cells (SOFCs) because of its high conductivity, resistance to reduction, good mechanical strength, and stability at high temperatures.[1] The key to this application is the high concentration of mobile anion vacancies created to charge-compensate for the introduction of Y^{3+} dopant onto the Zr^{4+} sites. YSZ is a solid solution series of the general formula $Zr_{1-x}Y_xO_{2-x/2}$, which has a fluorite structure in which the concentration of oxygen vacancies depends on the value of x. According to the ZrO_2−Y_2O_3 phase diagram,[2] Figure 1a, the cubic YSZ solid solution extends over the composition range $0 < x < 0.7$ at high temperatures. At lower x values, the solid solutions transform rapidly to tetragonal and/or monoclinic structures upon cooling. At higher x values, the cubic solid solutions should transform or precipitate secondary phases upon cooling, but transformation rates may be very slow. The coordination numbers of zirconium and yttrium, which are disordered, depend on x and are less than the ideal value of 8 in the fluorite structure.[3] The cation distribution may not be completely random, however; in composition x = 0.5, corresponding to the formula $Y_{0.5}Zr_{0.5}O_{1.75}$, there is a preference for a higher coordination number for yttrium of 7.2 compared to 6.8 for zirconium.[3] The composition x = 0.5 is sometimes referred to as a pyrochlore,[4] but diffraction data and crystal structure modeling[5] show little evidence of a pyrochlore structure apart from this indication of a nonrandom cation distribution.

The composition most widely used in SOFC applications with the highest oxide ion conductivity is x = 0.08 and is labeled as YSZ08 in this work.[1] At higher x, the oxygen vacancy concentration increases, but defect interactions are held responsible for mobile-ion trapping, leading to a reduction in the conductivity and an increase in the activation energy.[6] For instance, x = 0.5 has an oxide ion conductivity of 3.75×10^{-3} S cm^{-1} at 800 °C,[7] compared to 2.50×10^{-2} S cm^{-1} for YSZ08 used in SOFCs.[1]

For all oxide-ion-conducting solid electrolytes, the electrolytic domain is limited at low oxygen partial pressures, pO_2, by the onset of n-type electronic conduction and at high pO_2 by the onset of p-type conduction, as shown schematically in Figure 1b.[8] YSZ08 is generally regarded as stable down to a pO_2 value of 10^{-20} atm, which leads to its use as an electrolyte in contact with the anode and reducing atmospheres. Little information is available on the upper pO_2 limit of the electrolytic domain for YSZ08, probably because of the difficulty in achieving a wide range of pO_2 values greater than atmospheric pressure. Nevertheless, in the p-type region and using Kroger−Vink notation, it is assumed that the uptake of oxygen may occur by a mechanism summarized as

$$V_o^{\bullet\bullet} + \frac{1}{2}O_2 \rightarrow O_o^{x} + 2h^{\bullet} \quad (1)$$

Received: March 14, 2017

DOI: 10.1021/acs.inorgchem.7b00673
Inorg. Chem. XXXX, XXX, XXX−XXX

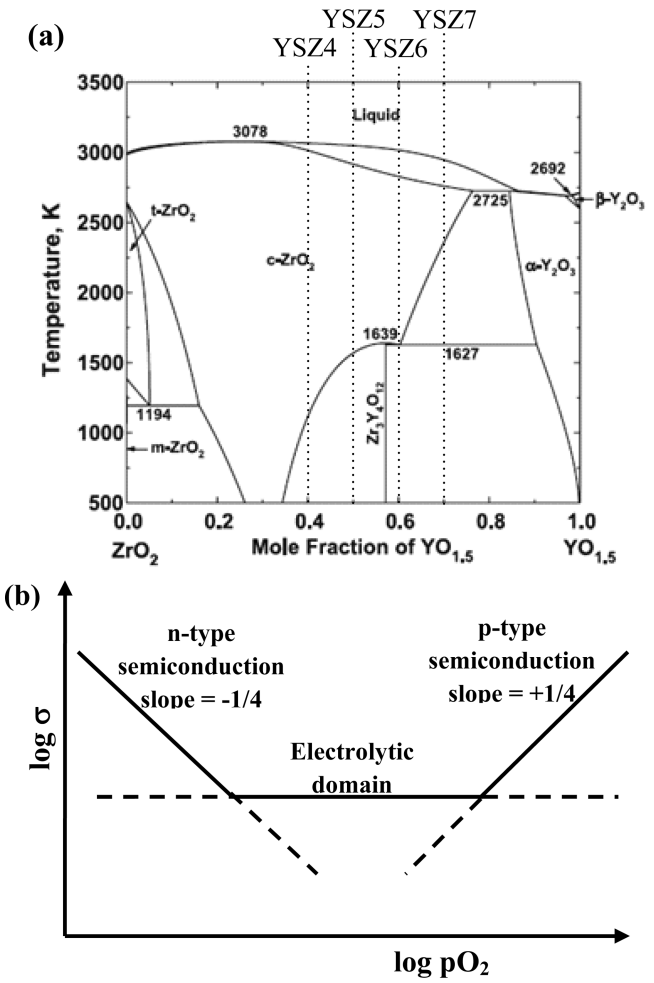

Figure 1. (a) Phase diagram of the ZrO_2–$YO_{1.5}$ system.[2] The compositions prepared in this work are indicated. (b) Schematic ionic and electronic conductivity domains as a function of pO_2, adapted from ref 8.

leading to a gradient of $+^1/_4$ in plots of log σ versus log pO_2. Usually, holes are assumed to be located on transition-metal ions, present as either controlled dopants or unavoidable impurities, but direct evidence for the site of the hole location seems to not be available.

Recently, Masó and West[9] demonstrated that electronic conduction is introduced into YSZ08 under the action of a small direct-current (dc) bias at high temperature in air. Similar conductivity changes were seen with acceptor-doped titanate perovskites including calcium-, zinc-, and magnesium-doped $BaTiO_3$[10−12] and calcium-doped $BiFeO_3$,[13] which all show enhanced conductivity with either an increase of pO_2 in the measuring atmosphere or the application of a small dc bias. The enhanced conductivity was attributed to the ionization of underbonded O^{2-} ions in the vicinity of acceptor dopants, leading to hole creation on oxygen, which, conceptually, is the same as the creation of O^- ions:

$$O_o^x \rightarrow O_o^\bullet + e' \quad (2)$$

The O^- ions are responsible for the enhanced electronic conductivity, which is p-type, because the ionized electrons have been immobilized at sample surfaces by participating in one, or more, of the equilibria

$$O_2(g) \leftrightarrow O_2(ads) \leftrightarrow O_2^- \leftrightarrow O_2^{2-}/2O^- \leftrightarrow 2O^{2-}(surface) \leftrightarrow 2O^{2-}(bulk) \quad (3)$$

The p-type conduction in the acceptor-doped titanate perovskites is thermally activated, which means that the holes are localized rather than delocalized in the valence band. Therefore, it is a logical step to refer to the holes localized on oxygen as O^- ions.

Although the conductivity of YSZ with $x = 0.08$ is not sensitive to pO_2 in atmospheres such as O_2, N_2, or air at atmospheric pressure, preliminary tests on compositions with higher x showed that their conductivity is, indeed, sensitive to pO_2. The present work reports a systematic study of the conductivity of YSZ with $0.4 < x < 0.7$ to determine the effects of pO_2 and dc bias on the electrical properties.

EXPERIMENTAL SECTION

Four compositions based on the general formula $Zr_{1-x}Y_xO_{2-x/2}$, with x = 0.4, 0.5, 0.6, and 0.7 and labeled YSZ4, YSZ5, YSZ6, and YSZ7, respectively, were prepared by a polymeric sol–gel procedure using $Y(OOCCH_3)_3{\cdot}H_2O$ (99.9%, Strem Chemicals) and $Zr(OCH_2CH_2CH_3)_4$ (70% Sigma-Aldrich) as precursors. All reagents were of analytical grade and were used without further purification. Absolute ethanol (Scharlab, 99.9%) was used as a solvent with the necessary amount of acetylacetone, acacH (99% Alfa Aesar), as a stabilizing agent for the zirconium alkoxide precursor. Zirconium alkoxide was dissolved in an ethanol–acetylacetone mixture (acacH:Zr molar ratio 4:1), the $Y(OOCCH_3)_3{\cdot}H_2O$ added, and the mixture stirred for 10 min, then transferred to a balloon flask, and heated at 70 °C for 72 h. A transparent gel formed and was dried in air under an IR lamp at room temperature for approximately 1 day. Finally, the dry gel was ground with an agate mortar and pestle, decomposed by heating at 5 °C min^{-1} to 500 °C, left at 500 °C for 1 h, and then heated to 1300 °C at a rate of 5 °C min^{-1} with a final hold at 1300 °C for 12 h. Powder samples were cooled, crushed, pressed into pellets of 5 mm diameter at 1 ton of uniaxial pressing, reheated at 1300 °C for 24 h, and cooled slowly inside the furnace. The four compositions chosen lie in the fluorite-structure phase field at high temperatures, as shown in Figure 1a. Pellet densities for all compositions were ∼85%.

The phase(s) present were analyzed by powder X-ray diffraction (XRD) using a Bruker D4 Endeavor diffractometer, Karlsruhe, Germany, with Cu Kα radiation. Data were collected by step scanning from $2\theta = 20$ to 70° with a step size of 0.03° and 6 s counting time at each step. The cubic lattice parameter was determined by least-squares refinement for reflections in the range $15 < 2\theta < 70$, using *WinXPow*, version 1.06 (Darmstadt, Germany). Scanning electron microscopy (SEM) images of the pellets were taken on a field-emission scanning electron microscope (JEOL 7001F), equipped with a spectrometer for energy-dispersion analysis of X-rays (EDX) from Oxford Instruments, using an acceleration voltage of 15 kV. The samples were deposited on an aluminum holder and coated with platinum.

For electrical property measurements, electrodes were fabricated on opposite pellet faces from platinum paste (Pt Ink 6082, Metalor, Barcelona, Spain), which was dried and decomposed by gradual heating to 900 °C. Samples with electrodes attached were placed in a conductivity jig and measured using an Agilent 4294A (Agilent, Madrid, Spain) analyzer over the frequency range of 40 Hz to 13 MHz and the temperature range of room temperature to 900 °C. Impedance data were corrected for overall pellet geometry and are reported in units of specific resistance (Ω cm) and capacitance (F cm^{-1}); data were not corrected for the geometry of the regions such as grain boundaries because this was not accurately known. Data were not corrected for the sample porosity. In order to avoid any effect of water, and therefore any possible proton conduction, impedance data were recorded in dry atmospheres. Measurements in atmospheres of different pO_2 values were carried out in a specially designed cell fitted with a built-in zirconia

DOI: 10.1021/acs.inorgchem.7b00673
Inorg. Chem. XXXX, XXX, XXX–XXX

probe (MicroPoas by SETNAG) next to the sample to measure the pO_2 value.

RESULTS

Pellets fired at 1300 °C for 24 h were ground and analyzed by XRD. All samples were single phase and were indexed on a cubic unit cell, space group $Fm\bar{3}m$, fully consistent with literature data. XRD data for x = 0.5 are shown in Figure 2a. There was no

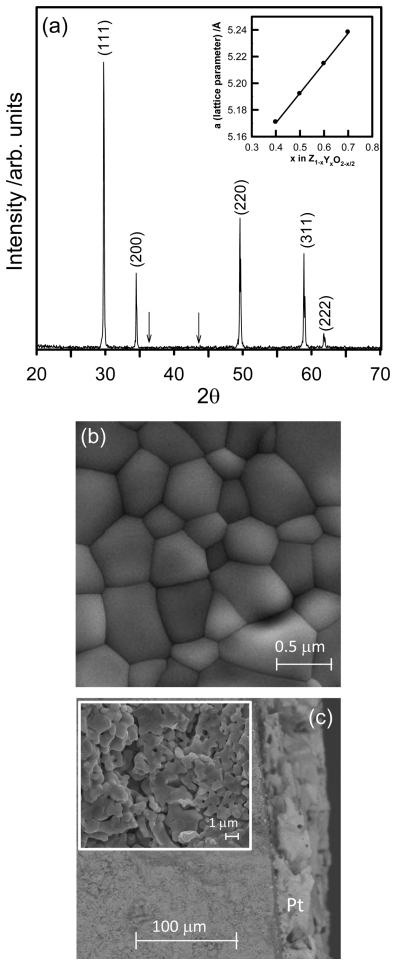

Figure 2. (a) XRD pattern and SEM images of (b) the pellet surface of YSZ5 sintered at 1300 °C and (c) the fracture surface of YSZ7 with the platinum electrode attached. Inset in part a: Variation in the lattice parameter with x. Inset in part c: Magnification of the YSZ7 microstructure of the fracture pellet.

evidence of a possible pyrochlore structure, whose XRD pattern is expected to contain extra peaks (indicated by arrows) at 2θ = 36.3 and 43.6 compared to the defect fluorite pattern.[14] Lattice parameters as a function of x (inset of Figure 2a) showed a linear increase with x.

The structure of the YSZ solid solution therefore contains a disordered mixture of Y^{3+} and Zr^{4+} distributed over the 8-coordinate sites of the fluorite structure, with some oxide ion sites vacant, depending on the composition x. From Figure 1a, the cubic solid solutions at 1300 °C are expected to form over the range $0.15 \leq x \leq 0.52$.[2,15,16] Our results showed single-phase cubic solid solutions over a more extensive range of compositions including x = 0.6 and 0.7. We do not know at present whether single-phase cubic solid solutions at these compositions are thermodynamically metastable, although clearly they are kinetically stable under the conditions of synthesis used here. These results may be consistent with the possibility of forming metastable phases by sol–gel synthesis.[17−20] A typical microstructure of the pellet surface for YSZ5 is shown in Figure 2b. Similar microstructures and grain sizes in the range 0.2–0.8 μm were observed for all compositions. An SEM image of a fracture surface through a pellet with the platinum electrode attached is shown in Figure 2c for sample YSZ7; the inset of this figure corresponds to a magnification of the YSZ7 microstructure and confirms the expected porosity. A homogeneous layer of the platinum electrode, in contact with the sample surface, is observed in this figure, showing that there is no penetration of the electrode into the interior of the sample. EDX mapping showed a homogeneous distribution of yttrium and zirconium, with no evidence of impurities for any of the compositions.

A typical set of impedance data, recorded in dry N_2 at 650 °C and presented in different formats, are shown in Figure 3 for a pellet of YSZ5 sintered at 1300 °C for 24 h with 85%density. A similar response was observed for all compositions. The impedance complex plane plots (a) show a broad, depressed arc at high frequencies and an inclined spike with some curvature at low frequencies. The total resistance obtained from the intercept of either the arc or the spike on the Z' axis had a value of ~20 kΩ cm. The Z''/M'' spectroscopic plots (b) show peaks at high frequencies that are much broader than expected for an ideal Debye peak, indicating some degree of probable electrical inhomogeneity in the sample but without clear separation of bulk and grain boundary impedances.

The plots of $\log C'/\log f$ (Figure 3c,d) for the same data at two temperatures, 650 and 823 °C, show evidence for a high-frequency plateau of the value ~10 pF, which corresponds to the limiting high-frequency permittivity of ~112. The C' values increase with decreasing frequency, with some evidence for a poorly resolved intermediate plateau at ~30 pF. This value is too small for it to represent a conventional grain boundary because it corresponds to a significant volume fraction of the sample. Instead, we attribute it to a combination of either a constriction grain boundary associated with the sample porosity and possible inhomogeneity in the distribution of the Y^{3+} dopant or a dipole orientation-related impedance such as that reported for YSZ08.[21] Further studies are in progress to understand the nature of this impedance.

With decreasing frequency, C' increases rapidly to reach a value of approximately 1 μF at 40 Hz and 823 °C (Figure 3d); this value is typical of ion blocking at a sample–electrode interface and the formation of a double-layer capacitance. The inclined spike shown in Figure 3a at low frequencies is attributed to the diffusion of oxygen molecules toward and away from sample–electrode interfaces, which therefore places a limit on the rate of oxygen-exchange reactions that occur during low-frequency measurements. Although this spike, attributed to a Warburg impedance, is not directly associated with oxide ion conduction, it is, nevertheless, an intrinsic component of redox reactions involving oxygen and is an indirect indication of oxide ion conduction. We therefore interpret the low-frequency impedance data to indicate that conduction is primarily by oxide ions but with the possibility of a small amount of electronic conduction (see later).

From data such as these, total sample resistances were obtained from intercepts of either the arc or the Warburg spike on the Z' axis and are shown as conductivity Arrhenius plots as a function of the reciprocal temperature in Figure 4; literature data for YSZ, x = 0.08,[22] are shown for comparison. The total

DOI: 10.1021/acs.inorgchem.7b00673
Inorg. Chem. XXXX, XXX, XXX−XXX

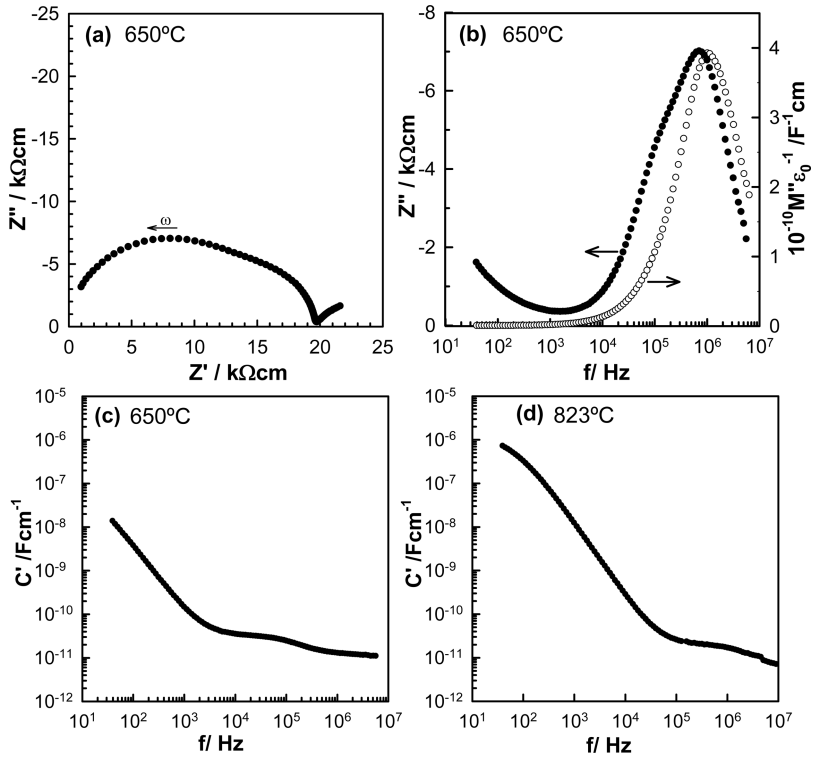

Figure 3. Impedance complex plane plots of (a) Z^* and (b) Z''/M'' and (c and d) C' spectroscopic plots at different temperatures for YSZ5. Measurements are in dry N_2; $\omega = 2\pi f$.

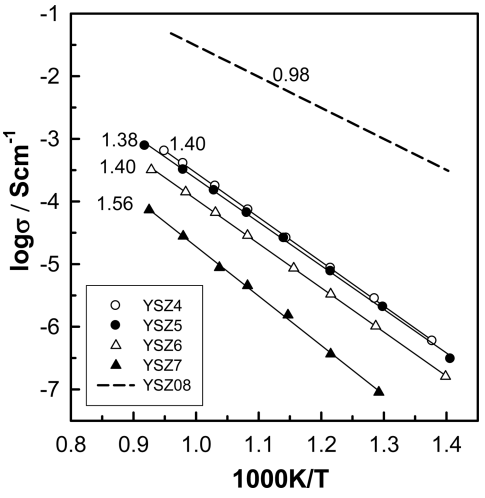

Figure 4. Arrhenius plots of the total conductivities for samples sintered at 1300 °C and measured in dry N_2. Error bars are within the size of the data points. The activation energies (eV), with errors in the range 0.02−0.05 eV, are shown beside each data set. The YSZ08 ceramic sintered at 1600 °C for 6 h is included for comparison.[22]

conductivity of YSZ solid solutions decreases with x and is 2−4 orders of magnitude lower than that of YSZ with $x = 0.08$. In addition, the activation energy increases with x. It is possible that the bulk conductivities are somewhat higher than the total conductivities shown in Figure 4 because either grain-boundary-constriction or dipole-reorientation impedances are included in the total resistance values; also, conductivities were not corrected for the sample porosity. The impedance measurements were obtained upon both cooling and heating, and the data were reproducible, showing linear behavior.

The data shown in Figures 3 and 4 were recorded in an atmosphere of dry N_2 with a pO_2 value of approximately 10^{-4} atm. Data are shown in Figure 5 for pellets of each composition measured in different atmospheres. Data were measured first in dry N_2 [$pO_2 \sim (1-2) \times 10^{-4}$ atm]; the atmosphere was then changed to dry O_2 ($pO_2 \sim 1$ atm) and the system allowed to stabilize for a few minutes before impedance data were collected in O_2. Two effects are seen in the impedance complex plane plots (Figure 5a−d), which were reversible upon switching between O_2 and N_2. First, the Warburg spike contracts greatly and becomes a small arc in O_2; second, the total sample resistance decreases. The effects were more noticeable with higher x compositions. It is most unlikely that these two phenomena could be attributed to changes in the oxide ion conductivity in the samples simply as a consequence of changing pO_2 in the measuring atmosphere.

Changes in the conductivity with pO_2 are widely used as an indication of extrinsic electronic conduction in materials because reactions such as eq 1 lead to changes in the electronic carrier concentration of either electrons or holes. We, therefore, interpret the data shown in Figure 5 to indicate the presence of p-type conduction when samples are measured in O_2 because chemisorption of oxygen with increasing pO_2 leads to hole creation (eq 1). This means that a certain amount of p-type electronic conduction[23,24] occurs in parallel with the preexisting oxide ion conduction. The electronic conduction must arise from reactions involving O_2 in the atmosphere. Equation 1 shows the creation of holes but gives no indication as to their location. Traditionally, holes are associated with transition-metal impurities, but we believe that a more likely location, at least in our materials, is underbonded oxide ions.

The loss of the Warburg spike is also attributed to the creation of a parallel electronic conduction pathway.[9] It is further emphasized in the capacitance data (insets in Figure 5a−d), in

DOI: 10.1021/acs.inorgchem.7b00673
Inorg. Chem. XXXX, XXX, XXX−XXX

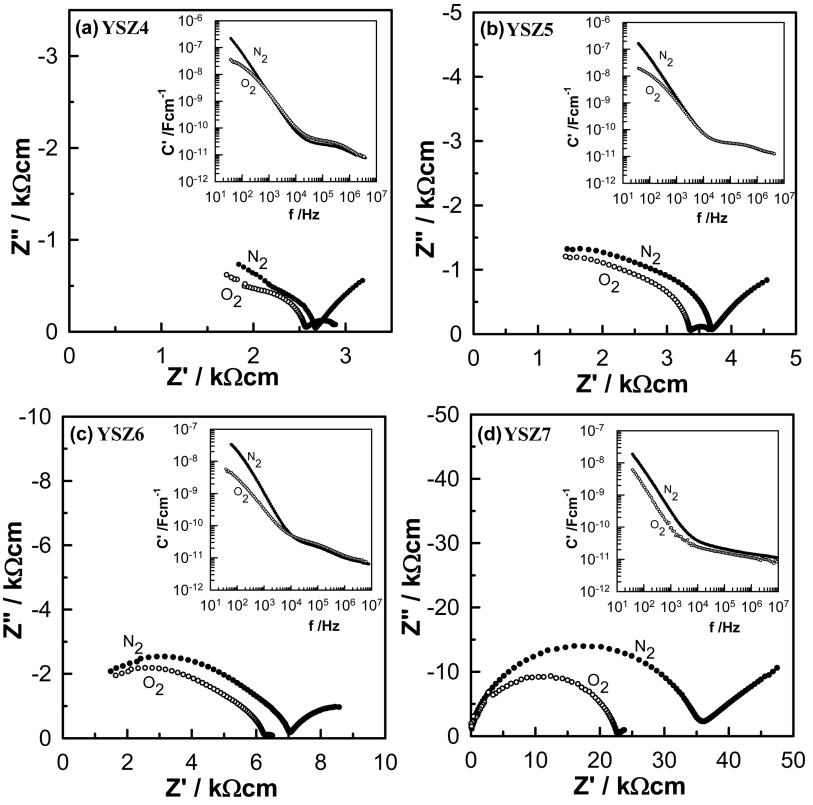

Figure 5. Impedance complex plane plots, Z^*, with C' spectroscopic plots as insets for all compositions measured in dry N_2 and O_2 at 750 °C.

which the large, high-valued low-frequency capacitance decreases because it is no longer associated specifically with charge transfer at the thin, double-layer interface.

Impedance data were sensitive to pO_2 over the complete temperature range studied, 500−850 °C, and are summarized in Arrhenius plots of the total conductivity for one composition, YSZ7, in Figure 6. The data recorded in O_2 are higher by a factor of 2−3 with a smaller activation energy and clearly must contain a contribution of both electronic and ionic conductivities. We do not know whether the data in N_2 also contain a small electronic component or whether they represent exclusively ionic conduction. These results show that, with reference to Figure 1b, samples YSZ4−YSZ7 in air at atmospheric pressure are in the crossover region between the electrolytic domain and p-type conduction. At present, we have not performed a detailed determination of the electronic transport number in our compositions, which would allow the contribution of each conduction mechanism to the electrical response to be determined as a function of the temperature, pO_2 and x. Different methods are reported in the literature to determine the electronic and ionic components of the conductivity.[9,25]

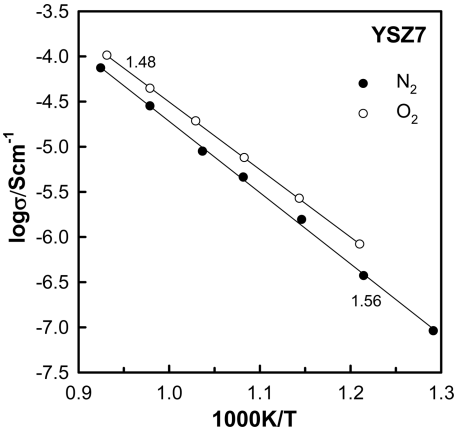

Figure 6. Arrhenius plots of the total conductivity for YSZ7 measured in dry N_2 and O_2. The activation energies (eV) are shown beside each data set.

The effect on the impedance data of the application of a small dc bias, in the range 0.5−2 V, was found to be very similar to that of increasing pO_2. A selection of results is shown in Figure 7 for YSZ7 and YSZ4. In Figure 7a, data are shown in N_2 and O_2 without an applied bias and in N_2 with 2 V bias. The data in O_2 and N_2 with 2 V bias are similar, and both show reduced total resistance and a much reduced Warburg spike. In Figure 7b, data are shown for dc bias in the range 1−10 V; a systematic decrease in both the sample resistance and Warburg impedance is observed.

The changes in the conductivity with changing pO_2 are not instantaneous but take a few minutes to reach the steady state, as shown in Figure 8 for YSZ5 at 750 °C. The sample was first equilibrated in N_2 for 24 h and the resistance measured as a function of time on switching to O_2. Once a steady state had been reached, the atmosphere was switched back to N_2; several minutes were needed to reach a steady state in both directions. Figure 8 therefore corresponds to a continuous time plot with a switch in the atmosphere at intermediate time.

DISCUSSION

The electrical properties of YSZ, $x = 0.4$−0.7, without application of a dc bias, are consistent with oxide ion conduction, as is, of course, widely recognized for YSZ08.[26] The conductivity is lower than that of YSZ08, which is usually used as a ceramic electrolyte

DOI: 10.1021/acs.inorgchem.7b00673
Inorg. Chem. XXXX, XXX, XXX−XXX

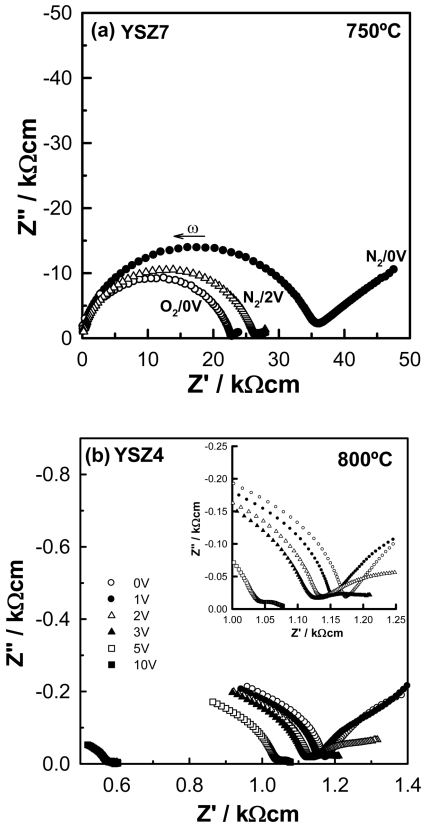

Figure 7. (a) Impedance complex plane plots for YSZ7 measured in dry N_2 and O_2 at 750 °C and with 2 V bias voltage in dry N_2. (b) Impedance complex plane plots for YSZ4 measured in dry N_2 after different bias voltages were applied at 800 °C.

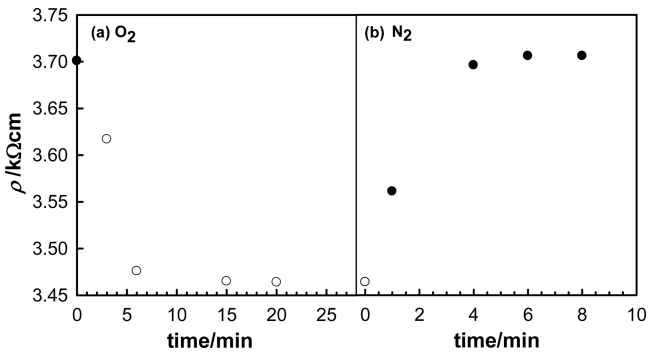

Figure 8. Time-dependent total resistivity for YSZ5 at 750 °C in dry (a) O_2 and (b) N_2.

in SOFC systems. Although the compositions prepared with higher x have a higher concentration of oxygen vacancies, the reduction in the ionic conductivity with increasing x is attributed to the trapping of oxygen vacancies in defect complexes associated with the Y^{3+} dopant; this is also consistent with the observed increase in the activation energy for ionic conduction in higher x compositions.[6]

YSZ08 is used as the ceramic electrolyte in SOFCs, in part because it is very stable to reduction. However, it has recently been shown that electronic conduction can be induced in YSZ08 by the application of a small bias voltage.[9] This causes YSZ08 to become a mixed conductor with, for instance, an electronic transport number, t_e, of 0.5 with 10 V bias at ~550 °C. The electronic conductivity is lost upon removal of the dc bias.

In the present study, we report a similar dependence of the conductivity on the dc bias but also show that the conductivity is sensitive to pO_2. The onset of the electronic conductivity is shown by two changes to the impedance data: first, the Warburg spike is greatly reduced and, second, the total sample resistance is reduced. Reversible changes of a similar nature are seen with both an increase in pO_2 and a dc bias. There is no evidence from the literature that YSZ08 is sensitive to an increase in pO_2, although it is sensitive to dc bias.[9] From the results presented here, the introduction of the electronic conductivity becomes easier with increasing x, and it seems highly probable, therefore, that YSZ08 itself will be sensitive to pO_2 at pressures just above 1 atm of O_2. This result has clear significance for the use of YSZ-based materials either in an O_2-rich atmosphere or in the presence of a bias voltage.

The sensitivity of the total sample conductivity to changes in pO_2 (Figure 5) is evidence that the electronic conduction mechanism is p-type. This was presumed, but not established, in the earlier YSZ results[9] and follows previous studies of acceptor-doped titanate perovskites that showed enhanced p-type conductivity with a dc bias. In those studies,[9−12] the mechanism of hole creation was attributed to the ionization of underbonded oxide ions associated with lower-valence acceptor dopants. The holes that are created are localized on oxygen, as O^- ions, and are responsible for the thermally activated p-type conduction. The Y^{3+} component of the YSZ solid solutions may be regarded also as an acceptor dopant in which Y^{3+} substitutes for Zr^{4+}; oxide ions in the immediate vicinity of Y^{3+} are effectively underbonded and can be readily ionized. The effect of increasing x is to increase the Y^{3+} concentration and, therefore, the concentration of underbonded oxide ions; this may account for the increased sensitivity to pO_2 that is seen with increasing x.

The chemisorption on sample surfaces that takes place with increasing pO_2 is a commonly used diagnostic for extrinsic conductivity and to distinguish p-type from n-type conduction. Using eq 1 to represent the chemisorption, electrons are removed from the sample, presumably close to the absorption sites, to form reduced oxygen species. In reality, several equilibria at sample surfaces may be involved, as indicated schematically in eq 3, giving rise to species such as superoxide O_2^-, peroxide O_2^{2-}, O^-, and finally O^{2-} ions, whose net negative charges are balanced by the holes that are created as lattice O^- ions. Several of these equilibria require electrons and, hence, with increasing pO_2, lead to an overall increase in the p-type conductivity, as shown in Figure 8. These processes commence at any part of sample surface exposed to the atmosphere.

Behavior similar to that seen with increasing pO_2 is observed upon application of a small dc bias, which, for voltages of 1−2 V, is below the probable decomposition voltage of the samples. This behavior may also be interpreted in terms of the equilibria shown in eq 3 because these equilibria are driven to the right-hand side by a positive bias, leading to the removal of electrons from the sample and an increase in p-type conduction. The positive electrode is therefore responsible for the observed conductivity changes, and there is no evidence of any opposite effect occurring at the negative electrode, which would lead to negative charge injection. Thus, if charge injection were to occur, this would lead to the onset of n-type conduction, as represented by the crossover region at low pO_2 shown in Figure 1b, in contrast to the observed p-type behavior. There are reported instances of blackening and electronic conduction in YSZ ceramics that can be attributed to charge injection from the negative electrode under highly reducing conditions. If changes to the sample do

DOI: 10.1021/acs.inorgchem.7b00673
Inorg. Chem. XXXX, XXX, XXX−XXX

occur at the negative electrode under dc bias, they are not directly responsible for the effects reported here. Thus, we also exclude the possibility of Schottky barrier formation and charge injection resulting from a reduction in the barrier height upon application of the dc bias.

CONCLUSIONS

There is huge interest in YSZ as the ceramic electrolyte for SOFC applications because, as well as its high oxide ion conductivity, it is very resistant to reduction; consequently, its "electrolytic window" extends down to very low partial pressures of oxygen before it shows the onset of n-type conduction. This work concerns the upper limit of the electrolytic window before the onset of p-type conduction.

Conductivity measurements in different atmospheres show that, with increasing yttrium content, YSZ compositions $x = 0.4-0.7$ are already at the crossover between electrolytic and p-type conduction upon switching between N_2 and O_2 atmospheres; a similar conclusion is reached from impedance measurements in the presence of a small dc bias and is attributed to the creation of holes on underbonded O^{2-} ions associated with the Y^{3+} acceptor dopant. We do not know the value of the activation energy for the electronic component in the p-type region, but it is probably nonzero, which means that the holes are localized on oxygen and not delocalized in the valence-band structure. The activation energy of YSZ7 in O_2, 1.48 eV, is somewhat less than that in N_2, 1.56 eV (Figure 6), and, therefore, the activation energy for p-type conduction is presumed to be less than that for oxide ion conduction.

These results are significant for several reasons:

First, they demonstrate that, depending on the yttrium content, YSZ samples may lose their exclusive oxide ion conductivity either in the presence of a small applied voltage or with increasing oxygen partial pressure. For samples of YSZ08 used in SOFC applications, the onset of p-type conduction is likely to occur at oxygen partial pressures close to, or slightly above, 1 atm.

Second, they demonstrate an alternative method by which electronic conductivity can be introduced into YSZ. Most focus in the literature is on the onset of possible n-type conductivity with either reducing atmospheres or decreasing pO_2, whereas we demonstrate the very easy introduction of p-type conductivity under near-ambient conditions and in the presence of small dc voltages.

Third, they highlight that the mechanism of hole creation must involve redox activity of underbonded oxide ions, which challenges the widely held belief that oxygen in oxides is present solely as the double-negative oxidation state. In high-purity chemicals such as those used here, there seems to be no other possibility for location of the holes.

Fourth, the ready introduction of p-type conductivity into YSZ-based materials may have significant consequences for their application as electronically insulating ceramics either in a high-pO_2 environment or in the presence of extraneous voltages.

AUTHOR INFORMATION

Corresponding Author

*E-mail: mir@uji.es.

ORCID

Héctor Beltrán-Mir: 0000-0002-7836-1602

Notes

The authors declare no competing financial interest.

ACKNOWLEDGMENTS

M.J., H.B.-M., and E.C. thank the Universidad Jaume I (Project UJI-B2016-38) and Ministerio de Economía, Industria y Competitividad (Project MAT2016-80410-P), for financial support. M.J. also thanks the Universidad Jaume I for a fellowship.

REFERENCES

(1) Stambouli, A. B.; Traversa, E. Solid oxide fuel cells (SOFCs): a review of an environmentally clean and efficient source of energy. *Renewable Sustainable Energy Rev.* **2002**, *6*, 433−455.

(2) Chen, M.; Hallstedt, B.; Gauckler, L. J. Thermodynamic modeling of the ZrO_2−$YO_{1.5}$ system. *Solid State Ionics* **2004**, *170*, 255−274.

(3) Zhang, Z.; Middleburgh, S. C.; De los Reyes, M.; Lumpkin, G. R.; Kennedy, B. J.; Blanchard, P. E. R.; Reynolds, E.; Jang, L. Y. Gradual Structural Evolution from Pyrochlore to Defect-Fluorite in $Y_2Sn_{2-x}Zr_xO_7$: Average vs Local Structure. *J. Phys. Chem. C* **2013**, *117*, 26740−26749.

(4) Panero, W.; Stixrude, L.; Ewing, R. First-principles calculation of defect-formation energies in the $Y_2(Ti,Sn,Zr)_2O_7$ pyrochlore. *Phys. Rev. B: Condens. Matter Mater. Phys.* **2004**, *70*, 054110-1−054110-11.

(5) Du, Q.; Zhou, G.; Zhou, J.; Jia, X.; Zhou, H. Enhanced luminescence of novel $Y_2Zr_2O_7$:Dy^{3+} phosphors by Li^+ co-doping. *J. Alloys Compd.* **2013**, *552*, 152−156.

(6) Kilner, J. A.; Steele, B. C. H. *Nonstoichiometric Oxides*; Academic Press, 1981.

(7) Kumar, M.; Raj, I. A.; Pattabiraman, R. $Y_2Zr_2O_7$ (YZ)-pyrochlore based oxide as an electrolyte material for intermediate temperature solid oxide fuel cells (ITSOFCs)-Influence of Mn addition on YZ. *Mater. Chem. Phys.* **2008**, *108*, 102−108.

(8) West, A. R. *Solid State Chemistry and its Applications*, 2nd ed.; Wiley, 2014.

(9) Masó, N.; West, A. R. Electronic Conductivity in Yttria-Stabilized Zirconia under a Small dc Bias. *Chem. Mater.* **2015**, *27*, 1552−1558.

(10) Masó, N.; Prades, M.; Beltrán, H.; Cordoncillo, E.; Sinclair, D. C.; West, A. R. Field enhanced bulk conductivity of acceptor-doped $BaTi_{1-x}Ca_xO_{3-x}$ ceramics. *Appl. Phys. Lett.* **2010**, *97*, 062907-1−062907-3.

(11) Beltrán, H.; Prades, M.; Masó, N.; Cordoncillo, E.; West, A. R. Voltage-Dependent Low-Field Bulk Resistivity in $BaTiO_3$:Zn Ceramics. *J. Am. Ceram. Soc.* **2010**, *93*, 500−505.

(12) Prades, M.; Masó, N.; Beltrán, H.; Cordoncillo, E.; West, A. R. Field enhanced bulk conductivity of $BaTiO_3$:Mg ceramics. *J. Mater. Chem.* **2010**, *20*, 5335−5344.

(13) Masó, N.; Beltrán, H.; Prades, M.; Cordoncillo, E.; West, A. R. Field-enhanced bulk conductivity and resistive-switching in Ca-doped $BiFeO_3$ ceramics. *Phys. Chem. Chem. Phys.* **2014**, *16*, 19408−19416.

(14) Zou, X.; Zhou, G.; Yi, H.; Zhang, G.; Wang, S. Fabrication of Transparent $Y_2Zr_2O_7$ Ceramics from Combustion-Synthesized Powders. *J. Am. Ceram. Soc.* **2011**, *94*, 1002−1004.

(15) Du, Y.; Jin, Z.; Huang, P. Thermodynamic Assessment of the ZrO_2-$YO_{1.5}$ System. *J. Am. Ceram. Soc.* **1991**, *74*, 1569−1577.

(16) Subramanian, M. A.; Aravamudan, G.; Subba Rao, G. V. Oxide pyrochlores - A review. *Prog. Solid State Chem.* **1983**, *15*, 55−143.

(17) Brinker, C. J.; Scherer, G. W. *Sol−Gel Science*; Academic Press: New York, 1990.

(18) Mackenzie, J. D. Unusual non-crystalline solids from gels in 2004. *J. Non-Cryst. Solids* **1985**, *73*, 631−637.

(19) Viazzi, C.; Bonino, J. P.; Ansart, F.; Barnabé, A. Structural study of metastable tetragonal YSZ powders produced via a sol−gel route. *J. Alloys Compd.* **2008**, *452*, 377−383.

(20) Beltrán, H.; Gómez, B.; Masó, N.; Cordoncillo, E.; West, A. R. Electrical properties of ferroelectric $BaTi_2O_5$ and dielectric $Ba_6Ti_{17}O_{40}$ ceramics. *J. Appl. Phys.* **2005**, *97*, 084104-1−084104-6.

(21) Hernandez, M. A.; West, A. R. Dipolar relaxation and impedance of an yttria-stabilised zirconia ceramic electrolyte. *J. Mater. Chem. A* **2016**, *4*, 1298−1304.

DOI: 10.1021/acs.inorgchem.7b00673
Inorg. Chem. XXXX, XXX, XXX−XXX

(22) Ren, P.; Masó, N.; Liu, Y.; Ma, L.; Fan, H.; West, A. R. Mixed oxide ion and proton conduction and p-type semiconduction in $BaTi_{0.98}Ca_{0.02}O_{2.98}$ ceramics. *J. Mater. Chem. C* **2013**, *1*, 2426−2432.
(23) Jamnik, J.; Maier, J. J. Treatment of the Impedance of Mixed Conductors Equivalent Circuit Model and Explicit Approximate Solutions. *J. Electrochem. Soc.* **1999**, *146*, 4183−4188.
(24) Lai, W.; Haile, S. M. Impedance spectroscopy as a tool for chemical and electrochemical analysis of mixed conductors: a case study of ceria. *J. Am. Ceram. Soc.* **2005**, *88*, 2979−2997.
(25) Huggins, R. A. Simple method to determine electronic and ionic components of the conductivity in mixed conductors. *Ionics* **2002**, *8*, 300−313.
(26) Brune, A.; Lajavardi, M.; Fisler, D.; Wagner, J. B., Jr. The electrical conductivity of yttria-stabilized zirconia prepared by precipitation from inorganic aqueous solutions. *Solid State Ionics* **1998**, *106*, 89−101.

DOI: 10.1021/acs.inorgchem.7b00673
Inorg. Chem. XXXX, XXX, XXX−XXX